Kinetic and structural characterization of whey protein aggregation in a millifluidic continuous process

Alice Vilotte, Hugues Bodiguel, Komla Ako, Deniz Gunes, Christophe Schmitt, Clément de Loubens

Kinetic and structural characterization of whey protein aggregation in a millifluidic continuous process

Alice Vilotte[a], Hugues Bodiguel[a,*], Komla Ako[a], Deniz Z. Gunes[b], Christophe Schmitt[b], Clément de Loubens[a]

[a] *Univ. Grenoble Alpes, CNRS, Grenoble-INP, Lab. LRP UMR 5520, F-38000 Grenoble, France*
[b] *Nestlé Research, Nestlé Institute of Material Sciences, Vers-Chez-Les-Blanc, Lausanne, CH-1000 26, Switzerland*

Abstract

Whey protein isolates (WPI) can be aggregated upon heating to create new functional properties (e.g. texture), which depend on aggregate size and structural properties. In industrial conditions, aggregates are obtained in continuous processes at high temperature (≥ 75°C) in few minutes. When studying the kinetics of WPI aggregation at high temperature and under flow, one major issue is to develop a process in which heat transfer does not limit aggregation. To this end, we used a down-scaling approach in which a WPI solution flows in a heated capillary tube. We show that this process makes it possible to study both the kinetics of aggregation after few seconds and its dependence with the mean shear rate in isothermal conditions. The size and mass of aggregates and protein conformation were characterized by small-angle X-ray scattering and resonant mass measurement for a single physico-chemical condition (pH 7.0, 10 mM NaCl, 92°C, 4 % w/w WPI) which led to sub-micrometric aggregates. Firstly, we report that the size of aggregates were three times larger than when produced in a test tube. Secondly, the size and mass of aggregates reached a steady-state value in a few seconds, whereas the kinetics of aggregation and denaturation had a characteristic time of few minutes. Thirdly, the shear rate had no significant effect on the size of the aggregates, or on the aggregation kinetics. We concluded that WPI aggregation at 92°C is limited by a step of nucleation, and that the fact that aggregates produced in test tube were smaller is due to a slower thermalization.

Keywords:
Heat-induced aggregation, Unfolding, Kinetics, Flow, SAXS

1. Introduction

Whey protein isolates (WPI) are of interest because of their nutritional and functional properties in food applications. Heat-induced aggregation coupled with the process conditions of whey proteins gives them new functional properties that can be used to impart the specific structural and physical properties of food products. Therefore, a thorough understanding and control of the aggregation process is required in order to design specific functional whey protein aggregates. The heat-induced aggregation process of whey protein (WP) is a complex multi-stage process but despite numerous studies, there are still many open questions that have not yet been resolved. (de la Fuente et al., 2002; Nicolai et al., 2011; Mezzenga & Fischer, 2013).

The rate of denaturation and aggregation of WPI depends on several factors such as pH, ionic strength, concentration and temperature. The measurement of apparent reaction rates of β-lactoglobulin and α-lactalbumin denaturation (the major component of WPI) on a wide range of temperature (70 - 150 °C) showed an abrupt change of the rate constant at 90 and 80°C, respectively (Dannenberg & Kessler, 1988). Subsequent studies have found that the overall aggregation process was limited by unfolding at low temperature (< 85°C) and aggregation reaction was the rate limiting step in the upper temperature range (> 100°C) (Verheul et al., 1998; Spiegel, 1999). Beyond kinetics studies, conformational changes of WPI have also been investigated to explain the rates of denaturation and aggregation (Relkin & Mulvihill, 1996; de Wit, 2009). While most of these studies did not make a distinction between unfolding limited from nucleation limited reaction, general mechanistic descriptions of heat-induced aggregation of WPI recognize an initiation, a propagation and a termination step (Roefs & De Kruif, 1994; Tolkach & Kulozik, 2007) by analogy with polymer radical chemistry (Roberts, 2007; Morris et al., 2009). More specifically, heat-induced aggregation of WPI involves the reversible self-association of two or more "reactive" monomers to form reversible non-native oligomers. The unfolding of these chains creates the smallest net irreversible aggregate, the nuclei, from which aggregates grow by covalent and/or noncovalent interactions and condensate. One main limitation of the kinetics studies cited above is that they based their analysis on the consumption of native proteins undergoing aggregation in order to measure the global kinetics constant, whereas it would also be valuable to measure the concentration of aggregated proteins to precisely determine the mechanism which limits the reaction. In this regard, X-ray scattering techniques can be used to simultaneously follow the concentration of native and aggregated proteins (Pérez et al., 2001) and also to gain insight on the structural properties of the aggregates (Moitzi et al., 2011).

The structure of aggregates can be modulated by varying

*hugues.bodiguel@univ-grenoble-alpes.fr

the balance between repulsive / attractive forces (Zuniga et al., 2010; Nicolai et al., 2011). One striking feature is the transition from fibrillar aggregates to microgels and fractal aggregates by changing the pH from 2.0 to 7.0 (Jung et al., 2008). The relationships of structural parameters of fractal aggregates with physico-chemical conditions and heat-treament have been well studied in regime of low temperature. Below 85°C, aggregation is limited by unfolding and takes place over several hours (Le Bon et al., 1999; Zuniga et al., 2010; Nicolai et al., 2011). According to Le Bon et al. (1999), the structure of fractal aggregates is independent of the concentration of β-lactoglobulin and the effect of the temperature is purely kinetic in the range 60 - 87°C. Zuniga et al. (2010) studied the effect of pH and holding time on the formation of thermally-induced β-lactoglobulin aggregates at 80°C and showed that the size of the aggregates saturated for a holding time ranging from 50 to 200 s, depending on the pH (6.0 - 6.8). However, these conditions are far from most industrial processes, in which a high temperature-short time UHT treatment is applied, reaching close to 140°C, and aggregation takes place over a few tens of seconds (Dissanayake et al., 2013). This rather fast aggregation is naturally combined with heat transfer in cases aggregation occurred in large-sized containers, such as batch reactors or test tubes. A simple way to increase the rate of heat transfer is to reduce the characteristic size of the sample down to the millimeter scale or below, as in a millifluidic continuous process (Dannenberg & Kessler, 1988). Coupling this kind of set-up with X-ray scattering techniques should also give us new insights into the kinetics of native and aggregated proteins, for example on the change of structural properties of the aggregates with the heating time. This kind of continuous process of agregation also offers an extra control parameter, which is the flow rate. It has been reported that the shear rate could affect the final aggregate size (Spiegel, 1999; Simmons et al., 2007; Wolz et al., 2016; de Guibert et al., 2020), but this control parameter has not been widely studied and conclusions are conflicting.

Our objective was to study the kinetics of growth of WPI (4% w/w, 10 mM NaCl) at high temperature (92°C) in a regime which should correspond to the transition between unfolding limited and aggregation-limited reactions (Dannenberg & Kessler, 1988; de la Fuente et al., 2002). Structural characterizations were done by X-ray scattering and resonant mass measurement and also covered the length scales of both the aggregates and the proteins. Both methods gave us complementary insights about aggregation and unfolding mechanisms. In the same way as Dannenberg & Kessler (1988) determined reaction rates of WPI at high temperature, we used a millifluidic continuous process to maximise the rates of heat transfer. This approach allowed us to accurately control the residence time, temperature history and shear rate.

2. Materials and methods

2.1. Materials and sample preparation

Whey protein isolate Prolacta 95 (batch 30916B) was purchased from Lactalis Ingredients (Bourgbarré, France). The composition of the WPI (Nx6.38) was (in g/100g powder wet basis): protein 88.5 (of which β-lacotglobulin 65%, α-lactalbumin 20%, soluble caseins 10% and almost 5 % of bovine serum albimin and immunoglobulin, ash 1.9, moisture 5.6, carbohydrates 0.14, fat 0.5). The mineral composition was (g/100g powder wet basis): Ca 0.35, Mg 0.06, Na 0.15, K 0.35, P 0.21, Cl 0.01.

WPI stock solution of 10% w/w was prepared by dispersing of the WPI powder in deionised water. Sodium Azide (0.02% w/w, Sigma-Aldrich CAS 26628-22-8) was added to the solution to prevent bacterial growth and gently stirred for 12 hours for complete dissolution of WPI powder. The stock solution was then dialyzed against salt-free deionised water containing 0.02 % w/w sodium azide. The concentration of the dialyzed solution of WPI was measured by UV absorption at 280 nm with an extinction coefficient of 1.186 L/g/cm. Finally, deionised water and sodium chloride was added to obtain a 4 % w/w WPI solution with an ionic strength of 10 mM, and pH was adjusted at 7.0 by the addition of sodium hydroxyde (1M).

2.2. Millifluidic continuous aggregation process

A continuous small scale process was designed to aggregate WPI solutions and decrease the characteristic time of heat transfer, so that aggregation occurred in isothermal conditions. The setup is presented in Fig. 1. WPI solution was injected at a constant flow rate Q with a syringe pump (low pressure neMESYS, Cetoni GmbH) at 22°C through a PTFE tube of internal and external diameter d_i = 0.81 mm (or d = 0.25 mm for the largest shear rates investigated, concerning the data displayed in Fig. 6) and d_e = 1.59 mm, respectively. The tube was immersed in a stirred and heated water bath at temperature T_∞ and fixed at 92°C for the entire study. The aggregates were collected for a few minutes in a tube immersed in ice and kept at 4°C until analysis.

We studied the effects of the mean residence time t of WPI in the tube and the mean shear rate $\dot{\gamma}$ on the aggregation process. Both parameters were varied by changing the tube length L and the flow rate Q. They are defined by

$$t = \frac{\pi d^2 L}{4Q} \tag{1}$$

$$\dot{\gamma} = \frac{64}{3\pi}\frac{Q}{d^3} \tag{2}$$

We investigated variations of t and $\dot{\gamma}$ from 20 s to 15 min and from 53 to 2666 s^{-1}. Consequently, Q and L ranged from 15 to 150 mL/h and 16.2 to 750 cm, respectively (d= 0.81 or 0.25 mm). The exact experimental conditions are given in the key of each figure. The flow was assumed to be laminar given that the range of Reynolds numbers, $Re = du/\nu$ was between 20.7 and 207, where $\nu = 3.2\times 10^{-7}$ m^2/s the kinematic viscosity of water at 92°C and $u = 4Q/\pi d^2$ the mean velocity in the tube.

The range of Peclet numbers investigated was always larger than 10^3. Thus, the effective diffusion coefficient of proteins along the longitudinal axis of the tube was greater than the molecular coefficient because of the parabolic velocity profile

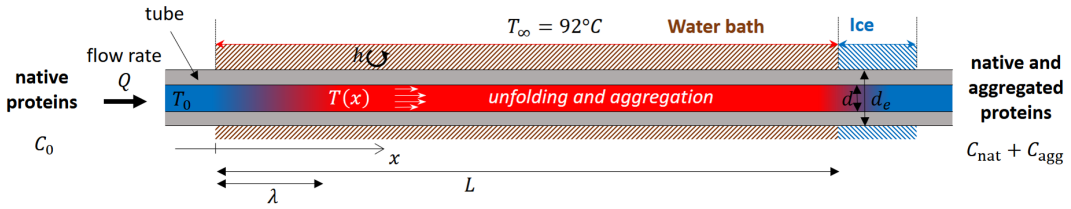

Figure 1: Diagram of the millifluidic continuous aggregation process. WPI solution flowed in 0.81 mm internal diameter tube at a flow rate Q and a temperature T_0. The tube was immersed in a heated water bath at temperature T_∞. From the time the tube was immersed ($x = 0$), the fluid temperature quickly rose along a characteristic length λ. The mean residence time t is directly proportional to the length L of the tube.

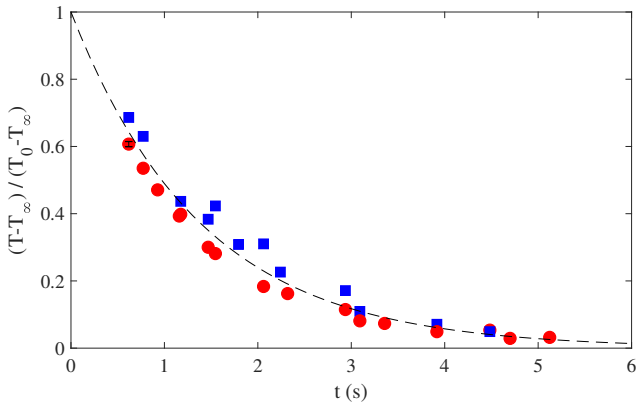

Figure 2: Reduced temperature $(T - T_\infty) / (T_0 - T_\infty)$ as a function of the residence time t (Eq. 5) in a tube of 0.81 mm internal diameter for various Q (60 to 300 mL/h) and L (10 to 30 cm). The temperature of the water bath, T_∞, was set at 80°C (squares) and 90°C (circles). The dashed line is the fit of Eq. 4 with the thermal characteristic time τ = 1.30 s (Eq. 5) that is independent of Q.

(i.e. Taylor-Aris dispersion, Taylor (1953); Aris (1956); Cussler (2009)), and we expect a dispersion of the residence time of the proteins around the mean value t. Based on the scaling laws of Chatwin (1970, 1977) and Latini & Bernoff (2001), we estimated that the standard deviation of the residence time ranged between ±11 s and ±3 min for mean residence times t of 20 s and 15 min, respectively.

The rate of heat transfer is of crucial importance in order to study aggregation at short times scales. A simple heat balance on an elementary volume of the liquid makes it possible to relate the temperature gradient along the tube length to the global heat transfer coefficient h accounting for internal and external convection as well as heat conduction through the tube walls. The mean temperature T at abscissa x from the point where the tube was immersed is given by

$$\frac{T(x) - T_\infty}{T_0 - T_\infty} = \exp\left(-\frac{x}{\lambda}\right), \tag{3}$$

where $\lambda = \frac{\rho c_p Q}{\pi d h}$ is the thermal entrance length and ρ and c_p are the density and specific heat of the aqueous solution. By substituting Eq. 1 in Eq. 3 with $x = L$, T can be expressed as a function of the residence time t

$$\frac{T(t) - T_\infty}{T_0 - T_\infty} = \exp\left(-\frac{t}{\tau}\right), \tag{4}$$

where the thermal characteristic time τ is given by

$$\tau = \frac{\rho c_p d}{4h}. \tag{5}$$

In the range of Re investigated ($Re \lesssim 1000$), the heat transfer coefficient is independent of the flow rate (Incropera et al., 2007), so that this characteristic time remains unchanged when the flow rate is varied.

This simple heat transfer model was tested experimentally by measuring the temperature at the outlet of the tube for various flow rates and tube lengths, Fig. 2. The data superimposes remarkably on an exponential decay law, as predicted, with a characteristic time of 1.30 s for the 0.81 mm tube. This strongly indicates that the model is adequate to describe the thermal history and that the heat transfer coefficient is independent of the flow rate. From this characteristic time value, the heat transfer coefficient is about $h \simeq 640$ W/K/m^2 and is similar to the coefficient that could be estimated assuming that transfers were limited by heat conduction through the tube walls. Importantly, this value of the thermal characteristic time allowed us to approximate the exponential function by a step function for times longer than a few tens of seconds. The heating rate was slower for the 0.25 mm tube, as it was thicker. From the thermal resistance of this tube, we estimate a thermal characteristic time of 3.38 s. This tube was only used for experiments at shear rates and residence time of more than 2000 s^{-1} and 60 s, respectively.

The residence time was limited to 15 min as the quantification of the fraction of remaining native-like WPI at this time showed that 5% of native WPI were remaining. This quantification was achieved according to the loss of solubility of the denaturated protein at pH 4.6 (Dannenberg & Kessler, 1988). Non-native like proteins and aggregates were precipitated by pH adjustment and the solution was then centrifuged at 20.000 × g for 20 min. The concentration of remaining native-like WPI in the supernatant was determined by UV absorption at 280 nm.

2.3. Test tube aggregation process

Aggregation under static conditions was induced in a polypropylene "test tube" of 5 mL (Eppendorf tube). This aggregation process is referred to as test tube process later on in this article and was used as a control with shear rates limited by natural convection. In this setup, isothermal conditions were reached after 3 minutes.

2.4. Small-Angle X-Ray Scattering

SAXS experiments were performed at ESRF (Grenoble) on beamline ID02 which offered an energy of 12.46 keV and a wide range of wave vector q, from 3×10^{-3} to 4 nm^{-1}. Samples were analyzed under static conditions in a glass capillary of 2 mm diameter. This method serves to measure the scattering of several samples within the same capillary, without handling it, and thus to accurately substract the contribution of the tube and the solvent from the scattering spectra. To minimize X-ray damage of the sample, the exposition time was set at 0.5 s. For each experimental condition tested, the background of the cell containing water and 4 spectra were acquired. Spectra of aggregates were obtained by averaging the 4 data sets and subtracting the background. For each condition, the sample was diluted up to a factor 100 with demineralized water to ensure that the spectrum could be assimilated to the form factor of the suspension of aggregates, i.e. the scattered intensity was linear with respect to the WPI concentration, in the whole range of wave vector. Diluting the sample with a solution of equivalent pH and ionic strength had no effect on the spectra (data not shown).

In particular, we focused on two ranges of wave vectors. In the Guinier regime ($q \ll 1/R_g$), the scattered intensity I of a dispersion of aggregates is given by

$$I(q) = \frac{I_0}{1 + q^2 R_g^2/3} \tag{6}$$

where R_g is the radius of gyration of the aggregates and

$$I_0 = K C_{\text{agg}} M_w, \tag{7}$$

where K is a constant, C_{agg} is the concentration aggregated proteins and M_w is their mass. I_0 and R_g were obtained by a least-square fitting of I as a function of $1/q^2$. Conformational changes in the structure of the proteins were detected in the high range of wave vector (0.5-3 nm^{-1}) by plotting Iq^2 as a function q^2 (Kratky plot, Pérez et al. 2001), which allowed us to follow the kinetics of denaturation.

2.5. Resonant Mass Measurement

The mass of individual aggregates M_w and its distribution were measured independently from SAXS analysis by resonant mass measurement (RMM, Archimedes, Malvern). A highly diluted dispersion was injected in a microfluidic channel with a micro-cantilever (Hi-Q Micro Sensor), for which the resonant frequency was calibrated. When a particle goes through the channel, the resonant frequency of the cantilever changes depending on the buoyant mass of the particle.

The buoyant mass (M_B) is proportional to the frequency shift Δf

$$M_B = \Delta f S \tag{8}$$

where S is the sensitivity of the resonator. The conversion of M_B into dry mass of aggregates M_w is based on the density of whey protein ρ_{WPI} (1.32 g/mL) and the density of water ρ_w (Weinbuch et al., 2013)

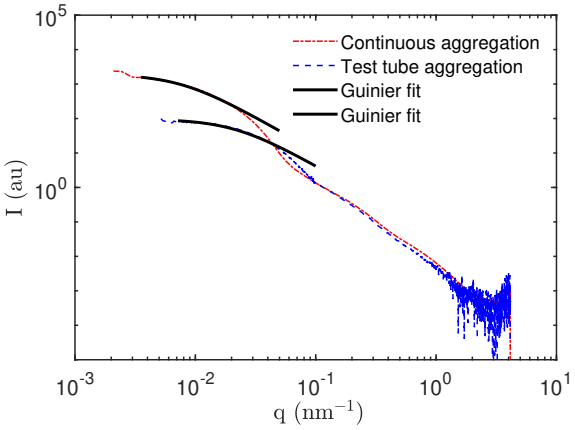

Figure 3: SAXS intensities $I(q)$ of the WPI aggregates obtained after 15 min of heat treatment at 92°C in a test tube (dashed line) and our millifluidic continuous process (dashed-dotted line), $\dot{\gamma}$ = 53 s^{-1}, d = 0.81 mm, Q = 15 mL/h, L = 7.3 m. Guinier fits (solid lines) gave R_g of 74 and 225 nm for test tube and continuous processes, respectively.)

$$M_w = \frac{M_B}{1 - \frac{\rho_w}{\rho_{WPI}}} \tag{9}$$

An archimedes device could detect particles with a mass of at least 4.5×10^{-16}g. A few thousands of aggregates were analyzed per sample, which enabled us to determine the probability density function (PDF) of aggregates mass weighted by their mass.

3. Results and Discussion

3.1. Comparison with aggregation in test tube

The main advantage of our millifluidic process of aggregation was to heat the solution of proteins at 92°C in few seconds and to control shear rates in laminar conditions (Figure 2). For a residence time of 15 min, we first compared the aggregates produced using the continuous millifluidic process ($\dot{\gamma}$ = 53 s^{-1}) and those using a more standard process in a test tube of 5 mL. In this second case, shear rates were limited to some natural convection and isothermal conditions were reached after 3 min.

The aggregates showed large differences on length scales larger than 10 nm, whereas there was no difference at smaller length scales (Fig. 3). For q larger than 0.1 nm^{-1}, the scattered intensities superimposed, meaning that the small scale structures of the aggregates were similar for both conditions. Moreover, quantification of the fraction of native WPI by pH adjustment to 4.6 (Delahaije et al., 2016) showed that the aggregation was almost complete at the end of the thermal treatment for both processes; the residual quantity of native WPI being only 5%. This statement was supported by the strong similarities of I in the q range of 0.5-2 nm^{-1}.

However, large differences were evidenced at lower q in the Guinier regime with striking differences in terms of radius of gyration R_g and scattered intensities I_0 (Eq. 6). R_g in test tube

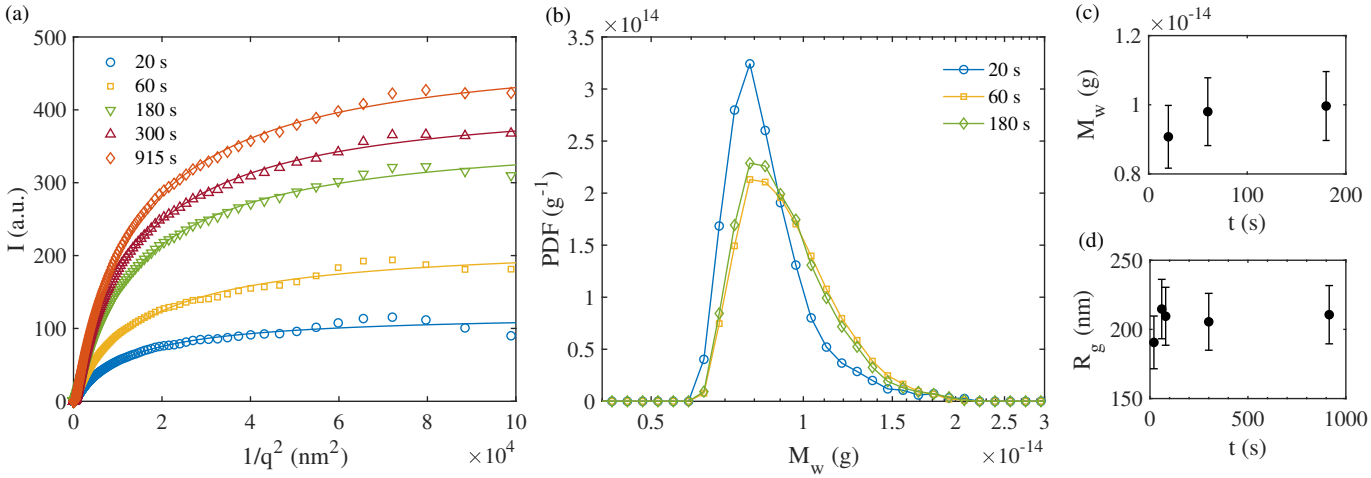

Figure 4: Kinetics of WPI aggregation. *a:* Guinier plot of SAXS intensity of aggregated WPI solutions for various residence times t at $\dot{\gamma}$ = 53 s^{-1} Solid lines are the fit of Guinier equation, Eq. 6. d = 0.81 mm, Q = 15 mL/h, L = 16.2 - 740 cm. *b:* Probability density function (PDF) of the mass of aggregates M_w for various t at $\dot{\gamma}$ = 32 s^{-1} as determined by RMM. d = 0.81 mm, Q = 9 mL/h, L = 10 - 87 cm. *c:* Mean value of M_w as a function of t, as determined by RMM. *d:* Radii of gyration R_g, which were obtained by the Guinier fit, as a function of t. Error bars represent ±10% of the mean value.

was 74 nm, i.e. three times lower than in the case of the millifluidic process (225 nm).

I_0 of aggregates obtained by millifluidic continuous process was 21 times bigger than the value of I_0 of aggregates obtained by test tube process. As C_{nat}/C_0 was about 0.05 at 15 min, we concluded that aggregation is almost complete for both processes after 15 min. Thus, the variation on the value of I_0 between the two conditions reflected directly the variations of mass of the aggregates ($I_0 \sim M_w$, Eq. 7). We inferred their relative density, $\rho^b/\rho^c \sim I_0^b/I_0^c \left(R_g^c/R_g^b\right)^3$, where ρ is the density in WPI of the aggregates and b and c refer to test tube and continuous conditions, respectively. We did not find any significant density differences between the two processes, $\rho^b/\rho^c \sim 1.3$. At first sight, this result does not fit with the findings of Spiegel (1999) of an increasingly compact aggregate structure with temperature. However, the thermal history was characterized by a slow heating across the range of temperature in our test tube, whereas isothermal conditions were achieved in the tubular process used by Spiegel (1999).

Two main differences between the two processes could be put forward to explain these contrasts: the thermal history and the fact that the continuous process involved a flow. The temperature strongly affects the various stages of WPI aggregation, their kinetics, their size (Spiegel, 1999; de Guibert et al., 2020; Petit et al., 2013) but also the protein conformations (Pérez et al., 2001; Tolkach & Kulozik, 2007). However, we did not observe significant differences in the high q range of the spectra between the two conditions, where protein conformation changes could be observed (see next section). In the continuous process, aggregation kinetics took place in a Poiseuille flow, which exhibited a gradient of velocity. Few studies showed that the shear rate could influence the size of large aggregates (de Guibert et al., 2020; Wolz et al., 2016; Simmons et al., 2007). The shear rate was also non-zero in the test tube due to natural convection, but should be smaller than the mean shear rate investigated in the small scale continuous process (53 s^{-1}). At this stage, it seemed difficult to further interpret the above result without the additional experiments that are detailed hereafter.

3.2. *Kinetics of aggregation in isothermal conditions*

The reaction and aggregate formation kinetics was studied using the millifluidic continuous process. We studied these kinetics along a range of residence time t (20 s - 15 min), for which the thermal history was approximated by a step function from 22 to 92°C (Figure 2).

R_g and M_w evolution of WPI aggregates with t for fixed values of $\dot{\gamma}$ (32 and 53 s^{-1}) were determined by SAXS and RMM, Figure 4. The results showed unambiguously that R_g and M_w remained almost constant from 20 s to 15 min of aggregation, with $R_g \simeq 205$ nm and $M_w \simeq 10^{-14}$ g. The slight increase of M_w remained in the order of the measurement uncertainty. We were also aware that the continuous process tended to average the tendencies over time due to diffusion and hydrodynamic dispersion in the longitudinal direction of the flow (see Section 2.2). The probability density functions (PDF) of M_w revealed that the suspension of aggregates had a polydispersity with a standard deviation of 30% of the mean value. Our results were in line with those of de Guibert et al. (2020) who studied WPI aggregation under similar physico-chemical parameters. The main differences were the thermal history and flow conditions, which were more complex (laminar and turbulent conditions) than those of this work. They also revealed the existence of a second population of WPI aggregates of smaller size by field-flow fraction. However, RMM could not detect masses smaller than 4.5×10^{-16} g. The aggregation number, which depicts the number of protein particles making up an aggregate, was about of $N_{\text{agg}} \simeq 3.3 \times 10^5$. The fractal dimension being 2 at

pH 7.0 (Gimel et al., 1994; Mehalebi et al., 2008; de Guibert et al., 2020), we estimated the size of the aggregates, as $R_g = b\sqrt{N_{\rm agg}}/6$, with b the size of the β-lactoglobulin (Moitzi et al., 2011), the main component of WPI. We found 220 nm, in very good agreement with the value estimated from the Guinier regime.

In contrast with the size, the scattered intensity at low q, I_0, increased progressively with t. Since the aggregate mass was roughly constant, I_0 was directly proportional to the concentration of aggregates $C_{\rm agg}$ (Eq. 7). Therefore, the aggregate concentration increased significantly from 20 to 915 s, by a factor of about 4.

This first set of results showed that the aggregate growth happened at short time scales (less than 20 s) and their size was limited, whereas WPI were continuously aggregated on time scales of few tens of minutes. These observations were consistent with previous studies (de Guibert et al., 2020; Zuniga et al., 2010; Roefs & De Kruif, 1994), except that at lower temperature the aggregates grew at time scales of a few minutes.

The kinetics of proteins unfolding was studied by focusing on the high q range of SAXS spectra, which is sensitive to the protein conformation. The Kratky plots displayed in Fig. 5 exhibited a significant change as a function of t. For the native proteins ($t = 0$), a bell-shaped curve was seen, whose the peak position corresponded to the length scale of β-lactoglobulin. The peak intensity decreased when the residence time increased. For the longest residence time (915 s), this peak was very weak. This bell-shape curve is a signature of a globular protein (Rambo & Tainer, 2011; Bernado & Svergun, 2012), and the decrease of its intensity reflects the unfolding of the proteins upon heating (Pérez et al., 2001). Taking advantage of this feature and the fact that the form factor is a linear combination of the form factors of the different states of the protein in solution (Pérez et al., 2001), i.e. native, partially unfolded and irreversibly aggregated, we estimated the progress of the unfolding process.

In the range 1-2 $\rm nm^{-1}$, and as evidenced in Fig. 5, all the spectra were described by a linear combination of the spectrum of the native protein solutions ($I_{\rm nat}$, at $t = 0$) and of the final spectrum (I_f, $t = 915$ s), i.e the presence of partially unfolded proteins was neglected,

$$I(t,q) = \alpha(t) I_{\rm nat}(q) + [1 - \alpha(t)]\, I_{agg}(q) \tag{10}$$

with $\alpha(t) = C_{nat}(t)/C_0$. The acid precipitation test carried out on the final solution (at $t = 915$ s) revealed that it contained about 5% of native proteins. Thus, $I_f = 0.95 I_{\rm agg} + 0.05 I_{\rm nat}$, where $I_{\rm agg}$ is the intensity of a fully aggregated solution. The remaining fraction of native proteins was inferred from the value of α for a given aggregation time, as

$$\frac{C_{\rm nat}(t)}{C_0} = 0.95\alpha(t) + 0.05. \tag{11}$$

The fraction of native proteins decreased in the first 60 s, a time at which half of the proteins were unfolded (Fig. 5). Note that the estimation of $C_{\rm nat}$ by the test of the loss of solubility of the denaturated protein at pH 4.6 was coherent with the values obtained by SAXS.

This kinetics of unfolding was compared with that of aggregated WPI, $C_{\rm agg}(t)$. Since the aggregate mass was approximately constant, the fraction of aggregated proteins was directly inferred from the time evolution of the low-q SAXS intensity I_0:

$$\frac{C_{\rm agg}(t)}{C_0} = 0.95\frac{I_0(t)}{I_0(t = 915s)}. \tag{12}$$

Note that this quantification of $C_{\rm agg}$ was independent of that of $C_{\rm nat}$, which was inferred from high-q SAXS intensity plot.

The symmetry between $C_{\rm agg}/C_0$ and $C_{\rm nat}/C_0$ is striking (Fig. 5). Moreover $(C_{\rm agg}(t) + C_{\rm nat}(t))/C_0$ varied by ±15% around 1 during the entire aggregation process. This clearly shows that the rate of protein unfolding was that of protein aggregation. This result highlights the self-consistency of our approach and confirms that WPI aggregation occurs as soon as a nucleus is present. it is worth mentioning that the above analysis in the high-q range assumes only two states for the protein conformation, which was an oversimplified picture. However, the fact that $(C_{\rm agg}(t) + C_{\rm nat}(t)) \simeq C_0$ justifies *a posteriori* this assumption.

The order of the reaction n is defined as $dC_{\rm agg}/dt = kC_{\rm nat}^n$, where k is the reaction rate constant, which is supposed to be a function of temperature and solvent composition. Reaction orders n were reported to vary between 1 and 2 (Dannenberg & Kessler, 1988; De Wit, 1990; Erabit et al., 2016; Wolz et al., 2016; Roefs & De Kruif, 1994; Phan-Xuan et al., 2011; Zuniga et al., 2010). From kinetic models of β-lactoglobulin that recognized that the rate of nucleation (initiation) is much smaller than the rate of propagation (aggregation), we expected a n of 1.5 (Roefs & De Kruif, 1994; Tolkach & Kulozik, 2007). $n = 1.5$ was also predicted theoretically for rapid aggregation theory of colloidal solutions (Smoluchowski, 1918). Our results were consistent with an order of 1.5 (subpanel in Fig. 5-b) and confirm that nucleation is the limiting step.

A simplified reaction scheme for the aggregation may consist in two main steps, the first one is a nucleation step, where one or a few (n_0) native proteins N undergo conformational change and irreversible association to form a precursor P for subsequent aggregation in aggregates A_i made of i proteins

$$\begin{aligned} n_0 N &\rightarrow P \\ P + N &\rightarrow A_{n_0+1} \\ A_{n_0+i} + N &\rightarrow A_{n_0+i+1} \end{aligned}$$

This scheme is that of a standard nucleation and growth process. It does not detail the initial conformational changes leading to the first irreversible precursor P, but since these are reversible with a very short charasteristic time (Roberts, 2007), they have limited impact on the aggregation scenario except concerning the dependency with initial concentration C_0, which is not studied here. It also ignores possible combinations between aggregates. To fully model the above results, this reaction scheme should involve a kind of termination step in order to limit the growth of the aggregates to a given size (Roefs & De Kruif, 1994; Roberts, 2007). The possible mechanisms are discussed hereafter.

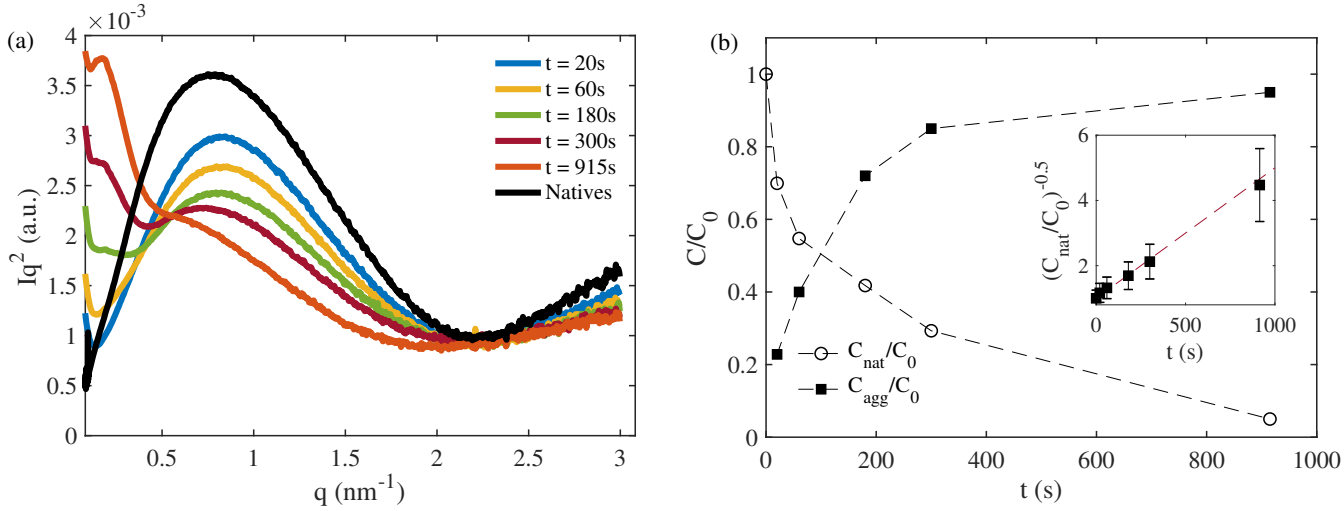

Figure 5: *a:* Kratky plots showing the change of WP conformation with the residence time *t*. . *b :* the fraction of native WP, C_{nat}/C_0 was determined from high q-range of spectra (∘, Eq. 10, 11) and was calculated from a linear combination of the spectra of natives and aggregated WPI in the q-range 1-2 nm^{-1} (dashed lines), see text for details. The fraction of aggregated WP, C_{agg}/C_0, was determined independently from the low q-range of spectra (■, Eq. 12). Dashed lines are guide for the eyes. In insert, kinetic plot $(C_{nat}/C_0)^{1-n}$ versus t with reaction order n= 1.5. $\dot{\gamma}$ = 53 s^{-1}, d = 0.81 mm, Q = 15 mL/h, L = 10 - 87 cm

The above detailed experimental results might be summarized as follows: (i) Denaturation and aggregation occured consequently, since intermediate states of WPI (i.e. unfolded but not aggreagted) were negligible at all times, (ii) Aggregates were formed within a few seconds, much faster than the global reaction rate, and their concentration kept growing over time with constant size and mass. The second one implied two features: on the one hand aggregation is not the limiting step and on the other hand there exists an additional mechanism which limits the growth of the aggregates when they have reached a given size. Other scenarios are not compatible with these two key observations. In particular, if aggregation was the limiting step, then the aggregate size would have increased significantly during the process.

We could only speculate on the scenario which limits the growth of the aggregates to a given size (for the studied experimental conditions, about 200 nm). Based on analogy with radical polymerisation chemistry, Roefs & De Kruif (1994) suggested that the polymerization process of β-lactoglobulin stopped when one reactive intermediate A_{n_0+i} reacted with another one forming an aggregate without a reactive sulhydryl group. Under this assumption, they predicted that $M_w \sim C_0^{0.5}$. Their reaction scheme was consistent with their kinetics of aggregation at low temperature (65°C). However, Zuniga et al. (2010) moderated this concept, as their experiments at 80°C insinuated that small molecular weight intermediates were cross-linked by disulfide bonds and formed larger aggregates via noncovalent bonding (e.g. by hydrophobic interactions). Competition between short-range depletion attraction and long-ranged electrostatic repulsion also leads to equilibrium clusters of finite-size whose number of aggregation N_{agg} is proportional to C_0 (Stradner et al., 2004; Campbell et al., 2005; Cardinaux et al., 2007). However, some of our preliminary results would invalidate the above-mentioned mechanisms as we found that R_g was constant for C_0 ranging from 0.4 to 4% w/w at 92°C and residence time t of 60 s, in agreement with Mehalebi et al. (2008); Phan-Xuan et al. (2011)(pH 7.0, no added salt, 85°C and $C_0 \leq 7$ g/L). Alternatively, our results could be explained by the mechanism introduced by Phan-Xuan et al. (2011) in which a self-stabilization effect could appear due to spontaneous increase of the pH during aggregate formation that should lead to an increase of their surface charge density and inhibits secondary aggregation. Similarly to the association of charged amphiphilic polymers (Zhulina & Borisov, 2012), counterions should be partly repelled from the aggregates and may lead to this electrostatic repulsion. At this stage, we have no experimental evidence that could validate or not one of these mechanisms. Additional studies varying the ionic force and the concentration of WPI would be interesting to test these various hypotheses.

3.3. Effect of shear rate

The flow rate Q was one of the important control parameters of the millifluidic continuous process that allowed us to increase the production rate, but also the mean shear rate $\dot{\gamma}$ (Eq. 2) in laminar conditions. The general picture depicted by previous studies is that shear rate could be a control parameter of the aggregate size. For low and moderate shear rate, the size should increase as the rate of collision between monomers and oligomers increases. At higher shear rates, the size should decrease as shear forces could break down the aggregates. An optimum could exist (Simmons et al., 2007; Wolz et al., 2016). However, this picture is not clearly established for thermal denaturation of proteins due to the difficulty of uncoupling thermal history from flow conditions (Erabit et al., 2016; de Guibert et al., 2020). We studied a range of shear rates $\dot{\gamma}$ which extended from 50 s^{-1} to 2.66×10^3 s^{-1} (Fig. 6). The comparison was made for an intermediate residence time t of 60 s for which one half

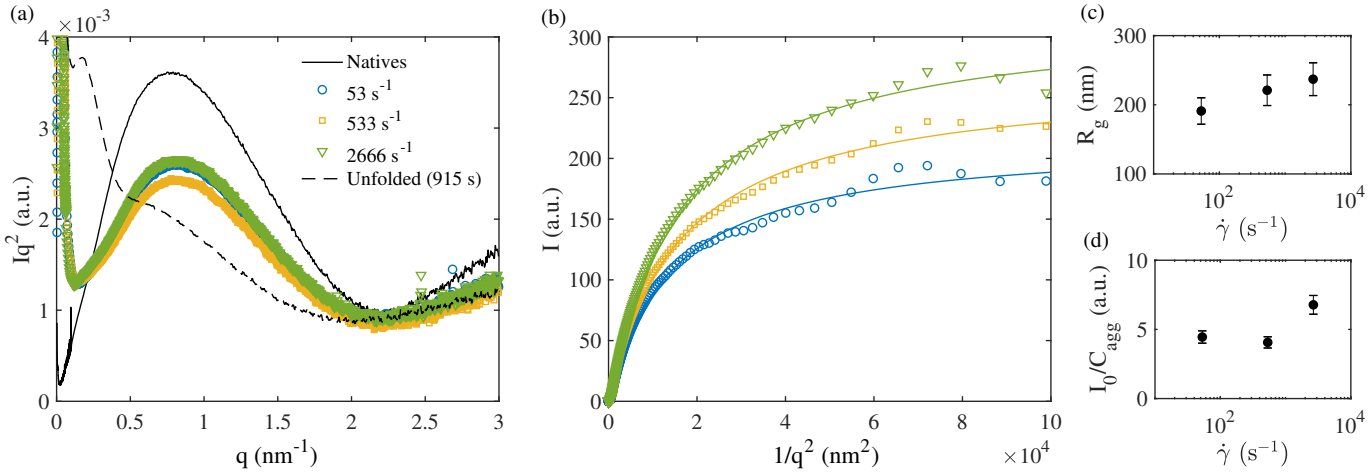

Figure 6: Effect of shear rate on denaturation and aggregation. *a:* Kratky plot showing the invariance of WP conformation for the different shear rates investigated for t = 60 s . *b:* Guinier plot of SAXS intensity for various shear rates at t = 60s. Solid lines are the fits using the Guinier equation (Eq. 6). *c:* Radii of gyration R_g as a function of $\dot{\gamma}$. *d:* I_0/C_{agg} as a function of $\dot{\gamma}$. $C_{\text{agg}} = 1 - C_{\text{nat}}$ was determined from the Kratky plot. d = 0.81 mm and 0.25 mm for $\dot{\gamma} = 2.5 \times 10^3 \text{s}^{-1}$, Q = 15 - 150 mL/h, L = 48.6 - 750 cm.

of native WPI were aggregated and so Kratky plots were sufficiently distinct from native and fully aggregated proteins. This particular choice had no major consequences since we reported that the structural properties of the aggregates (mass and size) did not significantly depend on the residence time.

The Kratky plots for the three shear rates investigated superimpose in the high-q range (Fig. 6-a). This feature showed unambiguously that the aggregation kinetics was not changed when $\dot{\gamma}$ was increased. For very high shear rates, the flow could influence the frequency of the collisions between reactants and thus increase the reaction rate. The relevant Péclet number for this effect is $\text{Pe} = \dot{\gamma} l^2/D$, where l is a characteristic distance between the considered reactants, which was of the order of 10 nm for the proteins, but significantly higher for the aggregates. For the highest shear rate tested, this Péclet number remained lower than unity ($\text{Pe} \simeq 0.2$), meaning that diffusion remained the dominant mechanism. It is thus not surprising that the shear rate did not influence the aggregation rate, provided that the nucleation stage is the limiting one.

In the Guinier regime, the data plots in Fig. 6-b exhibit a small trend. Both I_0 and R_g slightly increased when the shear rate was increased. R_g increased by about 10% for variations of $\dot{\gamma}$ of almost two orders of magnitude. From the values of I_0 obtained by the best Guinier fits and the value of $C_{\text{agg}} = 1 - C_{\text{nat}}$ inferred by a linear combination in the Kratky plots (see previous section and Fig. 5), we calculated the aggregate mass $M_w \sim I_0/C_{\text{agg}}$ (Eq. 7). M_w increased slightly with $\dot{\gamma}$, similarly to the radius of gyration. We were aware that these variations are of the order of magnitude of the measurement uncertainties, whereas $\dot{\gamma}$ varied by almost two orders of magnitude. We concluded that the shear rate had no significant influence on the aggregation or on the denaturation in isothermal conditions.

We returned our attention to the marked size differences between aggregates prepared using the millifluidc continuous process and the ones prepared in test tube (Fig. 3). We inferred that the shear rate was not responsible for this large increase of the aggregate size when switching from test tube to continuous process for the physico-chemical conditions investigated. The difference in heating rate was more likely to be responsible for the difference between test tube and continuous process. As in most processes, the scales are of a few millimeters, it is impossible to separate thermal from flow conditions. In light of the above results, our opinion was that some effects attributed to the influence of shear rate in previous studies (Simmons et al., 2007; Wolz et al., 2016) could be in fact attributed to large differences of thermal history. Additional studies varying the thermal history could be of interest to confirm that the latter could be used to tune the size of the aggregates.

4. Conclusions

In this paper, we studied the denaturation and aggregation of whey protein isolates under flow and at high temperature (92°C) for a single physicochemical condition leading to submicrometric aggregates (neutral pH, 10 mM NaCl,WPI 4 % w/w) with a well-controlled thermal history. We showed unambiguously that the size and mass of aggregates reached a steady state value within a few seconds, whereas the time scale associated with the kinetics of aggregation was of a few minutes. Moreover, we calculated from the Kratky plots the kinetics of consumption of native proteins, which was symmetrical to the kinetics of aggregated proteins. It means that partially unfolded proteins were virtually absent and WPI aggregated as soon as they are unfolded. The order of the reaction was consistent with 1.5, typical for rapid aggregation of proteins (Roefs & De Kruif, 1994; Tolkach & Kulozik, 2007). All these results lead us to conclude that the aggregation at 92°C is limited by the nucleation and there is a mechanism that limits the size of the aggregates. The underlying mechanism is an open issue (Roefs & De Kruif, 1994; Zuniga et al., 2010; Stradner et al., 2004;

Phan-Xuan et al., 2011). Different scenarios could be tested by varying protein concentration and / or ionic strength.

Moreover, we observed that the size of the aggregate and the denaturation is almost invariant with the shear rate (for variations covering almost two orders of magnitude) in isothermal conditions. We concluded that shear rate does not influence aggregation for the conditions tested and thermal history can be reasonably considered as responsible for the huge difference in terms of aggregate size between our millifluidic process and test tube conditions. This latter finding highlights the interest of studying growth of aggregates and unfolding with various thermal kinetics. The approach that we used in this work makes it possible to simultaneously characterize denaturation, nucleation and aggregation. We think it could be of great interest to extend it to other temperatures, especially higher ones which have been described as aggregation limited conditions (Dannenberg & Kessler, 1988).

Acknowledgements

The authors thank gratefully Theyencheri Narayanan (ESRF), Michael Sztucki (ESRF), William Chèvremont (LRP), Antoine Naillon (LRP), Mehdi Maleki (LRP) and Luis Carlos Morocho Rosero (LRP) for their technical support on the ID02 beamline of ESRF. We thanks also Frédéric Pignon (LRP) and Javier Perez (SOLEIL) for insingthfull discussions. LRP is part of the LabEx Tec 21 (Investissements d'Avenir – grant agreement ANR-11-LABX-0030) and Institut Carnot PolyNat (Investissements d'Avenir – grant agreement ANR-11-CARN-030-01).

Aris, R. (1956). On the dispersion of a solute in a fluid flowing through a tube. *Proc. Roy. Soc. A.*, *235*, 67–77.

Bernado, P., & Svergun, D. I. (2012). Structural analysis of intrinsically disordered proteins by small-angle x-ray scattering. *Molecular Biosystems*, *8*, 151–167.

Campbell, A. I., Anderson, V. J., van Duijneveldt, J. S., & Bartlett, P. (2005). Dynamical arrest in attractive colloids: The effect of long-range repulsion. *Physical Review Letters*, *94*, 208301.

Cardinaux, F., Stradner, A., Schurtenberger, P., Sciortino, F., & Zaccarelli, E. (2007). Modeling equilibrium clusters in lysozyme solutions. *EPL (Europhysics Letters)*, *77*, 48004.

Chatwin, P. C. (1970). The approach to normality of the concentration distribution of a solute in a solvent flowing along a straight pipe. *Journal of Fluid Mechanics*, *43*, 321–352.

Chatwin, P. C. (1977). The initial development of longitudinal dispersion in straight tubes. *Journal of Fluid Mechanics*, *80*, 33–48.

Cussler, E. L. (2009). *Diffusion: mass transfer in fluid systems*. Cambridge university press.

Dannenberg, F., & Kessler, H.-G. (1988). Reaction kinetics of the denaturation of whey proteins in milk. *Journal of Food Science*, *53*, 258–263.

De Wit, J. (1990). Thermal stability and functionality of whey proteins. *Journal of Dairy Science*, *73*, 3602–3612.

Delahaije, R. J., Gruppen, H., van Eijk-van Boxtel, E. L., Cornacchia, L., & Wierenga, P. A. (2016). Controlling the ratio between native-like, non-native-like, and aggregated β-lactoglobulin after heat treatment. *Journal of Agricultural and Food Chemistry*, *64*, 4362–4370.

Dissanayake, M., Ramchandran, L., Piyadasa, C., & Vasiljevic, T. (2013). Influence of heat and ph on structure and conformation of whey proteins. *International Dairy Journal*, *28*, 56 – 61.

Erabit, N., Ndoye, F. T., Alvarez, G., & Flick, D. (2016). Coupling population balance model and residence time distribution for pilot-scale modelling of β-lactoglobulin aggregation process. *Journal of Food Engineering*, *177*, 31–41.

de la Fuente, M. A., Singh, H., & Hemar, Y. (2002). Recent advances in the characterisation of heat-induced aggregates and intermediates of whey proteins. *Trends in Food Science & Technology*, *13*, 262 – 274.

Gimel, J. C., Durand, D., & Nicolai, T. (1994). Structure and distribution of aggregates formed after heat-induced denaturation of globular proteins. *Macromolecules*, *27*, 583–589.

de Guibert, D., Hennetier, M., Martin, F., Six, T., Gu, Y., Le Floch-Fouéré, C., Delaplace, G., & Jeantet, R. (2020). Flow process and heating conditions modulate the characteristics of whey protein aggregates. *Journal of Food Engineering*, *264*, 109675.

Incropera, F. P., Lavine, A. S., Bergman, T. L., & DeWitt, D. P. (2007). *Fundamentals of heat and mass transfer*. Wiley.

Jung, J.-M., Savin, G., Pouzot, M., Schmitt, C., & Mezzenga, R. (2008). Structure of heat-induced β-lactoglobulin aggregates and their complexes with sodium-dodecyl sulfate. *Biomacromolecules*, *9*, 2477–2486.

Latini, M., & Bernoff, A. J. (2001). Transient anomalous diffusion in poiseuille flow. *Journal of Fluid Mechanics*, *441*, 399–411.

Le Bon, C., Nicolai, T., & Durand, D. (1999). Growth and structure of aggregates of heat-denatured β-lactoglobulin. *International journal of food science & technology*, *34*, 451–465.

Mehalebi, S., Nicolai, T., & Durand, D. (2008). Light scattering study of heat-denatured globular protein aggregates. *International Journal of Biological Macromolecules*, *43*, 129–135.

Mezzenga, R., & Fischer, P. (2013). The self-assembly, aggregation and phase transitions of food protein systems in one, two and three dimensions. *Reports on Progress in Physics*, *76*, 046601.

Moitzi, C., Donato, L., Schmitt, C., Bovetto, L., Gillies, G., & Stradner, A. (2011). Structure of β-lactoglobulin microgels formed during heating as revealed by small-angle x-ray scattering and light scattering. *Food Hydrocolloids*, *25*, 1766–1774.

Morris, A. M., Watzky, M. A., & Finke, R. G. (2009). Protein aggregation kinetics, mechanism, and curve-fitting: A review of the literature. *Biochimica et Biophysica Acta*, *1794*, 375–397.

Nicolai, T., Britten, M., & Schmitt, C. (2011). β-lactoglobulin and wpi aggregates: Formation, structure and applications. *Food Hydrocolloids*, *25*, 1945–1962.

Pérez, J., Vachette, P., Russo, D., Desmadril, M., & Durand, D. (2001). Heat-induced unfolding of neocarzinostatin, a small all-β protein investigated by small-angle x-ray scattering. *Journal of Molecular Biology*, *308*, 721–743.

Petit, J., Six, T., Moreau, A., Ronse, G., & Delaplace, G. (2013). β-lactoglobulin denaturation, aggregation, and fouling in a plate heat exchanger: pilot-scale experiments and dimensional analysis. *Chemical Engineering Science*, *101*, 432–450.

Phan-Xuan, T., Durand, D., Nicolai, T., Donato, L., Schmitt, C., & Bovetto, L. (2011). On the crucial importance of the ph for the formation and self-stabilization of protein microgels and strands. *Langmuir*, *27*, 15092–15101.

Rambo, R. P., & Tainer, J. A. (2011). Characterizing flexible and intrinsically unstructured biological macromolecules by sas using the porod-debye law. *Biopolymers*, *95*, 559–571.

Relkin, P., & Mulvihill, D. M. (1996). Thermal unfolding of β-lactoglobulin, α-lactalbumin, and bovine serum albumin. a thermodynamic approach. *Critical Reviews in Food Science and Nutrition*, *36*, 565–601.

Roberts, C. J. (2007). Non-native protein aggregation kinetics. *Biotechnology and Bioengineering*, *98*, 927–938.

Roefs, S. P. F. M., & De Kruif, K. G. (1994). A model for the denaturation and aggregation of β-lactoglobulin. *European Journal of Biochemistry*, *226*, 883–889.

Simmons, M., Jayaraman, P., & Fryer, P. (2007). The effect of temperature and shear rate upon the aggregation of whey protein and its implications for milk fouling. *Journal of Food Engineering*, *79*, 517–528.

Smoluchowski, M. v. (1918). Versuch einer mathematischen theorie der koagulationskinetik kolloider lösungen. *Zeitschrift für physikalische Chemie*, *92*, 129–168.

Spiegel, T. (1999). Whey protein aggregation under shear conditions–effects of lactose and heating temperature on aggregate size and structure. *International Journal of Food Science & Technology*, *34*, 523–531.

Stradner, A., Sedgwick, H., Cardinaux, F., Poon, W. C., Egelhaaf, S. U., & Schurtenberger, P. (2004). Equilibrium cluster formation in concentrated protein solutions and colloids. *Nature*, *432*, 492.

Taylor, G. I. (1953). Dispersion of soluble matter in solvent flowing slowly through a tube. *Proc. Roy. Soc. A.*, *219*, 186–203.

Tolkach, A., & Kulozik, U. (2007). Reaction kinetic pathway of reversible and irreversible thermal denaturation of β-lactoglobulin. *Le Lait*, *87*, 301–315.

Verheul, M., Roefs, S. P. F. M., & de Kruif, K. G. (1998). Kinetics of heat-induced aggregation of β-lactoglobulin. *Journal of Agriculture and Food Chemistry*, *46*, 896–903.

Weinbuch, D., Zölls, S., Wiggenhorn, M., Friess, W., Winter, G., Jiskoot, W., & Hawe, A. (2013). Micro–flow imaging and resonant mass measurement (archimedes)–complementary methods to quantitatively differentiate protein particles and silicone oil droplets. *Journal of Pharmaceutical Sciences*, *102*, 2152–2165.

de Wit, J. (2009). Thermal behaviour of bovine β-lactoglobulin at temperatures up to 150°c. a review. *Trends in Food Science & Technology*, *20*, 27 – 34.

Wolz, M., Mersch, E., & Kulozik, U. (2016). Thermal aggregation of whey proteins under shear stress. *Food Hydrocolloids*, *56*, 396–404.

Zhulina, E. B., & Borisov, O. V. (2012). Theory of block polymer micelles: Recent advances and current challenges. *Macromolecules*, *45*, 4429–4440.

Zuniga, R., Tolkach, A., Kulozik, U., & Aguilera, J. (2010). Kinetics of formation and physicochemical characterization of thermally-induced β-lactoglobulin aggregates. *Journal of Food Science*, *75*, E261–E268.